Pressure distribution on a semi-circular concave surface impinged by a single row of circular jets.

Tejas Chafekar[1] Ranjit Kumar[2] Nishant Nayan[3], Vadiraj Katti[4] and S.V.Prabhu[5]
Department of Mechanical Engineering, Indian Institute of Technology, Bombay
svprabhu@iitb.ac.in, tejaschafekar@yahoo.co.in

Abstract

Experimental investigation is carried out to study the variation of pressure distribution on a concave semi-circular surface impinged by a single row of round multiple jets to study the effect of curvature (D/d = 4.25, 6.1 and 8.5), jet to plate distance (z/d = 1, 4 and 6), jet to jet distance (s/d = 2.4, 4 and 5.6) on the pressure distribution of the concave surface. Pressures are measured at three different angular locations namely 0^o, 30^o and 60^o by a micro manometer. Reynolds number of 20000 is maintained constant. Coefficient of pressure is reported for 15 different configurations obtained by changing jet to jet spacing, jet to plate spacing and curvature. It is observed that the coefficient of pressure reduces as the jet to plate distance increases for a given jet to jet distance and given curvature. Stagnation pressures are maximum for s/d = 4 whereas they decrease for s/d = 2.4 and 5.6 for a given jet to plate distance and a given curvature. Stagnation points are shifted away from the geometric centre of the jet in the flow direction (direction of flow of air in the jet tube). This shift increases with the increase in jet to plate distance (z/d). There are secondary pressure peaks in between two stagnation primary peaks which suggest an upwash. Secondary peaks vanish for lower jet to jet distances (s/d = 2.4). It is attributed to the mixing of the jets before they reach the surface. Actual mass flow rate through each jet exit is calculated. Coefficient of discharge is around 0.65 which is less than that reported for a flat plate in the literature. Hence, the resistance offered by concave curved surface is more than that offered by a flat surface.

Nomenclature

A_o	Throat area of venturi meter (m^2)
C_d	Coefficient of discharge
d	Diameter of jet (mm)
d_1	Diameter of the pipe upstream to the venture flow meter (mm)
d_o	Diameter of the venturimeter throat (mm)
D	Diameter of the curved surface (mm)
G_{jact}	Actual mass flow rate through each jet exit (kg/m^2)
G_{jideal}	Ideal mass flow rate through each jet exit (kg/m^2)
G_{javg}	Average mass flow rate through each jet exit (kg/m^2)
$\dot{m}$	mass flow rate (kg/s)
P	Atmospheric pressure (101325 Pa)
Po	Plenum pressure (Pa)
R	Universal gas constant (287 $Pa*m^3/(kg*K)$)
Re	Reynolds number ($\rho Vd/\mu$)
To	Room temperature (^oC)
V	Average velocity of jet (m/s)
X	Longitudinal distance along the axis of curved surface
Xn	Jet to jet distance (mm)
z	Distance between curved surface and jet tube (mm)
β	(d_o/d_1)
ρ_a	Density of air (kg/m^3)
ρ_w	Density of water (kg/m^3)
μ	Viscosity of air ($Pa\ s$)
θ	Angular position of pressure taps with respect to the jet direction (deg.)

Introduction

Impinging jets have received considerable research attention due to their inherent characteristics of high rates of heat transfer. Various industrial processes involving high heat transfer rates apply impinging jets. Few industrial processes which employ impinging jets are drying of food products, textiles, films and papers; processing of some metals and glass and cooling of gas turbine blades and outer wall of the combustion chamber; cooling

of electronics equipments. Chupp *et al.* [1] has studied the influence of Reynolds number (*Re*), jet to plate spacing (*z/d*), jet to jet pitch (*s/d*) and curvature (*D/d*) on the heat transfer distribution in a semi-circular concave surface impinged by single line of circular jets. They suggested the following correlations for the stagnation point heat transfer and average heat transfer.

$$Nu_{stag} = 0.44 Re^{0.7} \left(\frac{s}{d}\right)^{-0.8} \exp\left[-0.85 \left(\frac{l}{d}\right)\left(\frac{d}{s}\right)\left(\frac{d}{D}\right)^{0.4}\right] \quad (1)$$

$$Nu_{avg} = 0.63 Re^{0.7} \left(\frac{s}{d}\right)^{-0.5} \left(\frac{d}{D}\right)^{0.6} \exp\left[-1.27 \left(\frac{l}{d}\right)\left(\frac{d}{s}\right)^{0.5}\left(\frac{d}{D}\right)^{1.2}\right] \quad (2)$$

This correlation is valid for the following range of parameters: $3000 \geq Re \leq 15000$, $4 \geq s/d \leq 16$, $1 \geq z/d \leq 10$ and $1.5 \geq D/d \leq 16$.

Jusionis [2] studied the influence of gas flow rate, the distance of the jet exhaust holes from the model skin and the angle of inclination of the jet exhaust holes on the heat transfer distribution on concave enclosed surface impinged by multiple jets. They suggested a correlation for average Nusselt number based on Reynolds number, jet to plate spacing, jet to jet pitch and curvature of the concave surface. Metzger *et al.* [3] investigated the heat transfer characteristics of concave cylindrical surfaces impinged by single line of circular jets. Heat transfer coefficient was measured using a transient response of a thermal sensor made of aluminum with a thermocouple embedded in it. They suggested a correlation for maximum Nusselt number based on Reynolds number, jet to plate spacing, jet to jet pitch and curvature of the concave surface. Metzger *et al.* [4] experimentally studied the heat transfer characteristics of impingement into cavities which model the cooled leading edges of gas turbine engine airfoils. The influence of elongated leading edge was to decrease the overall heat transfer. Bunker and Metzger [5] conducted experimental investigation to measure local heat transfer distribution in scale down models of turbine blade impingement cooled leading edge regions. Cooling was provided by a single line of equally spaced multiple jets aimed at the leading edge apex and exiting the leading edge region in the chordwise direction. Combinations of variations in jet Reynolds number, airfoil leading edge sharpness, jet pitch to diameter ratio and jet nozzle to apex travel distance were covered in this study. Results indicated that the general increase in heat transfer with approximately the 0.6 power of jet Reynolds number, increase in heat transfer with decreasing leading edge sharpness as well as with decreasing nozzle to apex distance and increase in spanwise average heat transfer with decreasing jet pitch to diameter ratio.

Ramakumar and Prasad [6,7] conducted experimental and computational investigations to study the flow characteristics from multiple circular jets impinging on a concave surface. The experiments were performed with 30:1 scaled up model, mimicking the leading edge zone of a gas turbine nozzle guide vane. The parameters varied were jet Reynolds number (*Re* = 2850 -28476), jet height to diameter ratio (*z/d* = 1, 4 and 6), number of rows (1 and 5) and intra jet distance to diameter ratio (*s/d* = 2.7 and 5.4). A Finite volume based CFD code (Fluent) with the *k-ω* SST model for turbulence closure was used for the analysis. The jet fountain, upwash and entrainment were identified in the flow domain. The numerically obtained decay of center line velocity and the pressure distribution on the concave target plate were corroborated with the experimental data. Secondary peaks and negative pressures obtained in the experiments were reproduced in the computational studies.

Review of the literature suggests that little information is available on the flow distribution of single row impinging jets on concave semi-circular surface. Hence, the objective of the present experimental work is to investigate the pressure distribution on the concave surface impinged by a single row of circular jets. The parameters which are varied in this study are jet to plate spacing (*z/d* = 1, 4.2 and 6), jet to jet distance (*s/d* = 2.4, 4, 5.6), curvature (*D/d* = 4.25, 6.1 and 8.5) at a constant Reynolds number of 20000 and at angular positions of 0^o, 30^o and 60^o.

Experimental Setup and procedure

A schematic layout of test facility is as shown in Fig. 1. Air is supplied to the air plenum of test section by an air compressor through a calibrated venturi flow meter. Air filter and pressure regulator are installed upstream of the venturi flow-meter to filter out the air and to maintain the downstream pressure at a desired value. The flow rate is controlled by two needle valves, one on the each side of the venturi flow meter. The function of the upstream needle valve is to allow cool air to flow until the compressor has built up enough pressure in the reservoir. The flow rate is actually controlled by the downstream needle valve. Metered air is supplied to the test section through the supply jet-tube.

Figure 2a shows the isometric view of the test section. Figure 2b shows the location of the jet tube and the pressure taps with respect to the curved surface Figure 2c gives the dimensional details of

the holes used for pressure measurement. A target concave surface of 85 *mm* diameter (*D*) and thickness 8 *mm* is fixed normal to the impinging air jets. The jet tube has a single row of circular holes of constant diameter (*d*). The jets are positioned so as to impinge centrally on the semi-circular concave target surface. There are 81 pressure taps of 1 *mm* diameter each drilled on the surface. These pressure taps are placed at three angular locations of 0^o, 30^o and 60^o, along the longitudinal directions. Figure 2c gives the geometrical details of the concave surface. The protruding ends of the holes in the atmosphere are attached to a steel tube which is then attached to a flexible tube that can be plugged into a micro-manometer (Furness Controls Model FCO332-3W (±500 Pa) scaled ±20 mm of water, Supply 9-36V) to measure the static pressure on the surface. If the pressures are more than 20 *mm* of water, they are measured through a separate single tube manometer.

The air stream is made to enter the plenum. The jet of air strikes the concave surface. The direction of flow of air is shown in Fig. 1. Experiments are performed to investigate the pressure distribution on the concave surface impinged by a single row of circular jets. Experiments are performed for each combination of jet to plate distance (*z/d*) and diameter ratio (*D/d*) as mentioned above. Specific geometric configuration is represented in the form (*D/d, s/d, z/d) i.e.,* a configuration convention (8.5, 4, 1) represents a row of jets with diameter ratio *D/d* = 8.5, jet to jet distance (*s/d*) of 4 and jet-to-plate spacing of *z/d* = 3.0. Table. 1 summarizes all the experiments performed.

Data Reduction

The coefficient of pressure (*Cp*) is calculated as the ratio of the static pressure (gauge) at a given location on the concave semi-circular surface to the velocity head at the jet exit.

$$C_P = \frac{P - P_\infty}{0.5\rho V^2} \qquad (1)$$

where *Cp* = Coefficient of pressure, *P* = Static pressure at the surface, P_∞ =Atmospheric pressure, ρ = Density of air at 30^oC, *V* = Velocity of jet at exit. Maximum uncertainty in the measurement of coefficient of pressure is around 5 %.

Results and discussion

Experimental investigation is carried out to study the variation of pressure distribution on a concave semi-circular surface impinged by a single row of round multiple jets to study the effect of curvature (*D/d* = 4.25, 6.1 and 8.5), jet to plate distance (*z/d* = 1, 4 and 6) and jet to jet distance (*s/d* = 2.4, 4 and 5.6) on the pressure distribution of the concave surface. Pressures are measured at three different angular locations namely 0^o, 30^o and 60^o for a constant Reynolds number of 20000.

Influence of curvature (*D/d*) and jet to plate distance (*z/d*) for a given jet to jet distance (*s/d* = 4), on the pressure distribution.

Figures 4, 5 and 6 show the variation of coefficient of pressure with *X/Xn* for curvature (*D/d*) of 4.25, 6 and 8.5 respectively. For each *D/d* three jet to plate distances (*z/d*) of 1, 4 and 6 are shown at a constant jet to jet distance of *s/d* = 4. Pressure variation of each configuration is reported for three angular locations of 0^o, 30^o and 60^o. It is observed that maximum pressure (stagnation pressure) occurs at 0^o and its value decreases as the *z/d* is increased for a given *D/d*. Stagnation points are shifted away from the geometric centres of the jets in the flow direction (direction of flow of air in the jet tube). It is observed from Fig. 4 that the shifts in stagnation pressure increase with increase in *z/d*. For lower curvature of *D/d* = 4.25 the shifts for *z/d* = 1, 4 and 6 are *X/Xn* = 0.06, 0.37 and 0.56 respectively. From Fig. 5 it is observed that the shifts for *D/d* = 6.1 at *z/d* = 1, 4 and 6 are around *X/Xn* of 0.07, 0.25 and 0.37 respectively. However from Fig. 6 it is observed that the shifts are around 0.12, 0.25 and 0.37 respectively for higher curvature of *D/d* = 8.5. Thus it may be concluded that the amount of shift in stagnation pressure increases with increasing jet to plate distance. It is speculated that the jet exits at an angle to the jet tube instead of it exiting in perpendicular direction. The shift in the stagnation pressures can be attributed this phenomenon. Figures 4, 5 and 6 also show the presence of secondary peaks. These are due to the upwash as reported by Ramkumar and Prasad [7]. It is also observed from these figures that the secondary peaks do not lie exactly in between two stagnation peaks. They are shifted in the flow direction (direction of flow of air in the jet tube) by an amount of *X/Xn* = 0.08 and 0.12 for *z/d* = 4 and 6 respectively, for all curvatures. Thus the amount of shifts in the secondary peaks increase with jet to plate distance and are not sensetive to change in curvature. The shifts can be attributed to the phenomenon as shown in Fig. 11.

It is observed that the values of *Cp* for angular locations of 30^o and 60^o are much less than those at 0^o. As the angle increases, the pressure variation in the streamwise direction decreases. It is observed from Fig. 4, that for *z/d* = 4 and 6, the peak pressures at 30^o are nearly equal to those at 0^o. Figure 12 depicts the speculated phenomenon resulting in the rise in the pressure. As *z/d* is increased the jet cone might be reaching the pressure tap at an angular location of 30^o, thus increasing the pressure at this angular location.

It is observed that the stagnation pressures for each jet at higher curvature (D/d = 8.5) is constant for all jet to plate distances and lower curvatures (D/d = 4.25 and 6.1) at lower z/d of 1. However, for lower curvatures (D/d = 4.25 and 6.1) and higher jet to plate distances (z/d = 4.0 and 6.0), there is a decrease in the stagnation pressures along the flow direction.

Influence of jet to jet distance (s/d) for a given curvature (D/d = 6.1) and jet to plate distance (z/d), on the pressure distribution.

Figures 7, 8 and 9 show the effect of variation of jet to jet distance on the pressure values. In Figure 7 the pressure distribution at different angular locations for a jet to jet distance of 2.4 for various values of z/d is shown. It is observed that for all the jet to plate distances the variation in stagnation pressures with X/Xn is negligible. It is also observed that secondary peaks vanish as jet to jet distance decreases. This is attributed to the mixing of the two jets before reaching the surface as shown in Fig. 13. It is also observed that the value of pressure at 30^o approaches the stagnation value as the jet to plate distance increases. This can be attributed to the same phenomenon as discussed above. The same phenomenon is observed for (4.25, 4, 4) and (4.25, 4, 6) configurations. For higher jet to plate distances the value of pressures at 30^o and 60^o increases with the increase in X/Xn.

Figure 8 shows the variation of pressure with X/Xn at different angular locations for a jet to plate distance of 5.6. Unlike for shorter jet to plate distances (s/d = 2.4) secondary peaks are observed between two stagnation peaks. It is observed that for z/d = 1 the stagnation pressures are constant while at higher jet to plate distances their values decrease with increase in X/Xn. At higher jet to plate distances shifts are also observed to increase and the pressures at 30^o are seen to approach the stagnation pressures.

Figure 9 depicts the effect of change in jet to plate on the value Cp. It compares the values of Cp for different jet to jet distances for a particular value of z/d. It is observed that for all jet to plate distances the stagnation pressures for s/d = 4 are maximum and the decrease for s/d = 2.4 and 5.6. The decrease in the stagnation pressure for lower jet to plate distances can be attributed to the mixing of the two jets before reaching the curved surface as depicted in Fig. 13a.

Conclusions

Experimental investigation is carried out to study the variation of pressure distribution on a concave semi-circular surface impinged by single row of round multiple jets to study the effect of curvature (D/d = 4.25, 6.1 and 8.5) and jet to plate distance (z/d = 1, 4 and 6) jet to jet distance (s/d = 2.4, 4 and 5.6) on the pressure distribution on the concave surface. Pressures are measured at three different angular locations namely 0^o, 30^o and 60^o at a constant Reynolds number of 20000. Following conclusions are reported from the present study.

- The value of pressures at an angular location of 0^o is much higher than the values at 30^o and 60^o. The stagnation pressures decrease as the jet to plate distance is increased for a fixed curvature. For higher jet to plate distances the value of stagnation pressure also decreases along the flow direction.
- For a particular curvature (D/d) the stagnation pressure are not obtained exactly at the geometric centers. They are shifted towards right. This is attributed to the fact that, the jets, while exiting are not perpendicular to the axis of the concave surface. The shifts are more for higher jet to plate distances.
- It is observed that there is no significant effect of the change of curvature (D/d) on the values of peak pressures for a particular jet to plate distance (z/d). The secondary peaks are not exactly in the middle of two stagnation peaks. These are shifted towards right along the flow direction, and the amount of shift increases with increasing z/d.
- The stagnation peaks for D/d = 6.1 and a particular z/d is maximum for a jet to plate distance of 4. It decreases for s/d = 2.4 and 5.6.
- For higher curvatures and higher jet to plate distances, the values of pressures at 30^o approach the stagnation pressure values.

References

1. Chupp R. E, Helms H. E, Mc Fadden P. W., Brown T. R., "Evaluation of Internal Heat-transfer Coefficients for Impingement-cooled Turbine Airfoils", J. Aircraft, Vol 6 No. 3, (1969) 203-208
2. Jusionis V.J., "Heat Transfer from Impinging Gas Jets on an Enclosed Concave Surface", J. Aircraft, (1970) 87-88
3. Metzger D. E., Yamshita T., Jenkins C.W., "Impinging Cooling of Concave Surfaces with Line of Circular Air Jets", J. Engg. for Power, (1969) 149-158
4. Metzger D. E., Baltzer D.E., Jenkins C.W., "Impingement Cooling Performance in Gas Turbine Airfoils Including Effects of Leading Edge Sharpness", J. Engg. for Power, July, (1972) 219-225

5. Bunker R.S., Metzger, D.E. "Local heat transfer in internally cooled turbine airfoil leading edge regions. Part I: impingement cooling without fillm coolant extraction", ASME J. of Turbomachinery 12 (1990) 451-458
6. RamaKumar B.V.N, Prasad, B.V.S.S.S., "Experimental and Computational Study of Multiple Circular Jets Impinging on a Concave Surface", Proceedings of NCFMFP2006, 33rd National and 3rd International Conference on Fluid Mechanics and Fluid Power, I.I.T., Bombay, India
7. RamaKumar B.V.N, Prasad, B.V.S.S.S., "Computational flow and heat transfer of a row of circular jets impinging on a concave surface", Heat Mass Transfer, DOI 10.1007/s00231-007-0274-3

Table. 1

Sr. No.	*D/d*	*z/d*	*s/d*	*Θ*	*Re*	Number of jets
1	4.25	1	4	0°, 30°, 60°	20000	5
2	4.25	4.2	4	0°, 30°, 60°	20000	5
3	4.25	6	4	0°, 30°, 60°	20000	5
4	6.1	1	4	0°, 30°, 60°	20000	7
5	6.1	4.2	4	0°, 30°, 60°	20000	7
6	6.1	6	4	0°, 30°, 60°	20000	7
7	8.5	1	4	0°, 30°, 60°	20000	9
8	8.5	4.2	4	0°, 30°, 60°	20000	9
9	8.5	6	4	0°, 30°, 60°	20000	9
10	6.1	1	2.4	0°, 30°, 60°	20000	11
11	6.1	4.2	2.4	0°, 30°, 60°	20000	11
12	6.1	6	2.4	0°, 30°, 60°	20000	11
13	6.1	1	5.6	0°, 30°, 60°	20000	5
14	6.1	4.2	5.6	0°, 30°, 60°	20000	5
15	6.1	6	5.6	0°, 30°, 60°	20000	5

Fig. 1 Schematic layout of experimental setup

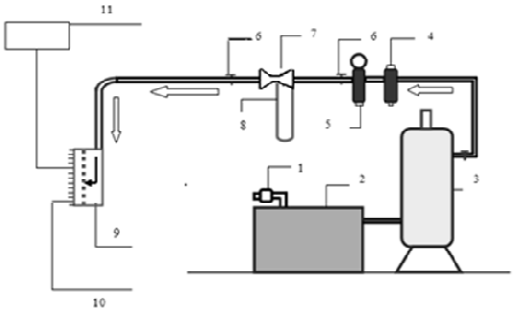

1) Air filter 2) Air compressor 3) Air receiver 4) Air filter 5) Pressure regulator

6) Needle valves 7) Venturi Flow meter 8) Manometer 9) Test section

10) Pressure taps 11) Micro-manometer

Fig. 2 Details of the test section

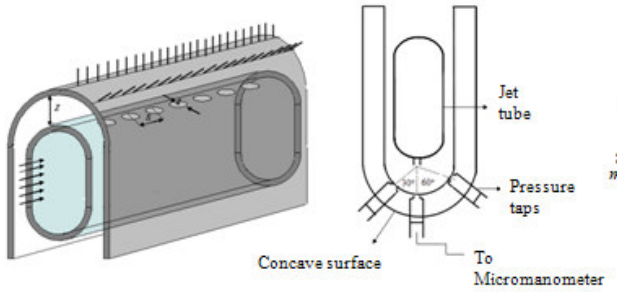

Fig. 2a Test Section

Fig. 2b The concave surface

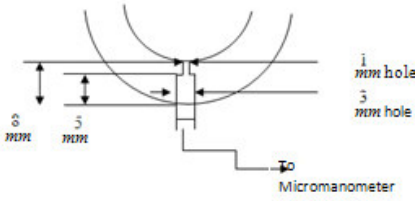

Fig. 2c Details of the concave surface

Fig. 3 Photographs of the test section

Fig. 3a The semi-circular concave surface

Fig. 3b The jet tube

Fig. 4 Coefficient of pressure (*Cp*) variation with dimensionless length (*X/Xn*) for *D/d* = 4.25 and *s/d* = 4.0 at a *Re* = 20000

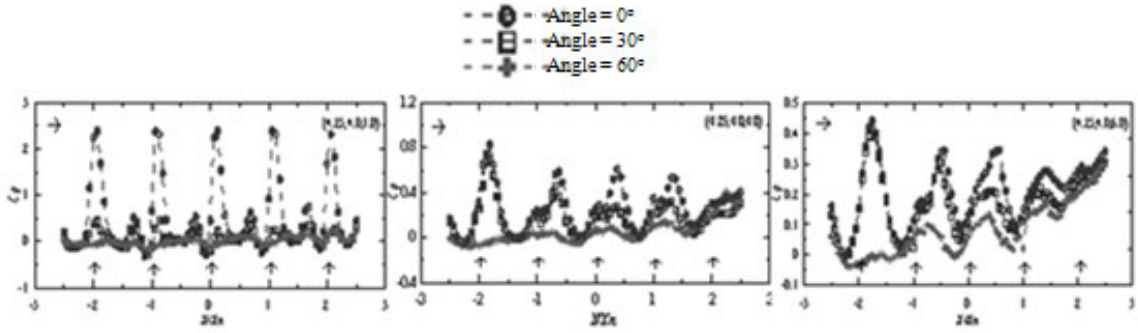

Fig. 5 Coefficient of pressure (*Cp*) variation with dimensionless length (*X/Xn*) for *D/d* = 6.1 and *s/d* = 4.0 at a *Re* = 20000

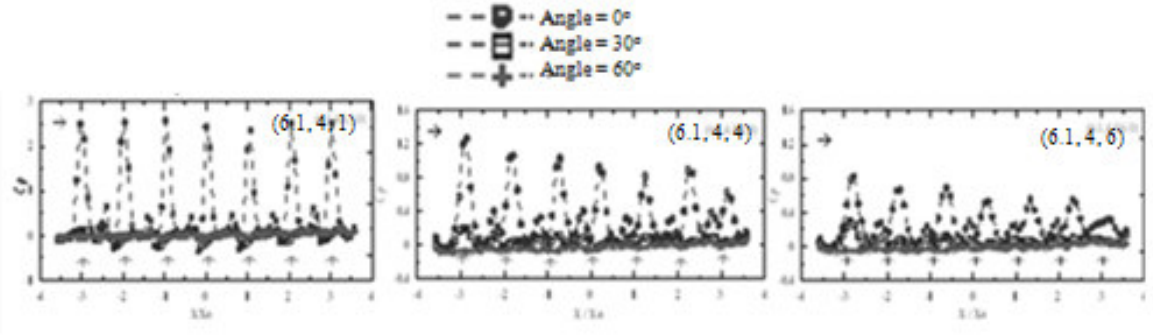

Fig. 6 Pressure coefficient (*Cp*) variation with dimensionless length (*X/Xn*) for *D/d* = 8.5 and *s/d* = 4.0 at a *Re* = 20000

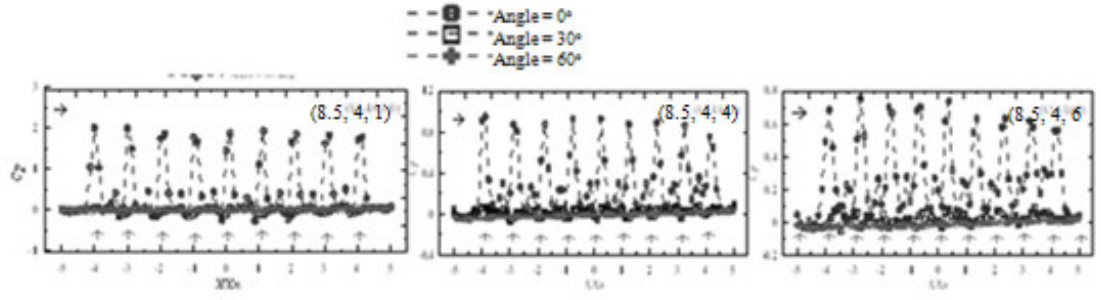

Fig. 7 Coefficient of pressure (*Cp*) variation with dimensionless length (*X/Xn*) for *D/d* = 6.1 and *s/d* =2.4 at a *Re* = 20000

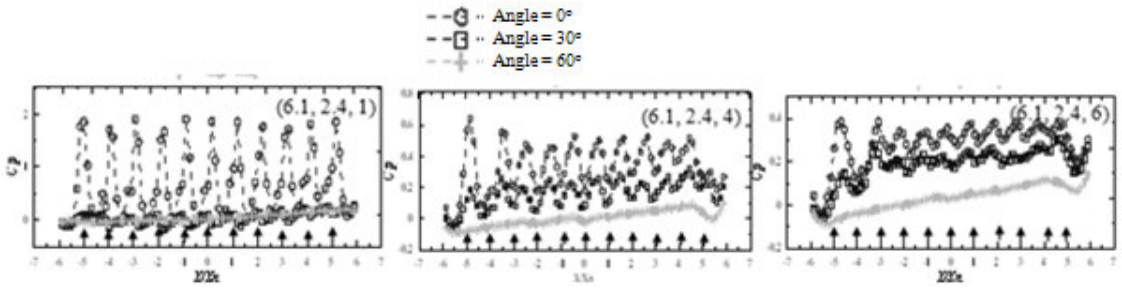

Fig. 8 Coefficient of pressure (*Cp*) variation with dimensionless length (*X/Xn*) for *D/d* = 6.1 and *s/d* = 5.6 at a *Re* = 20000

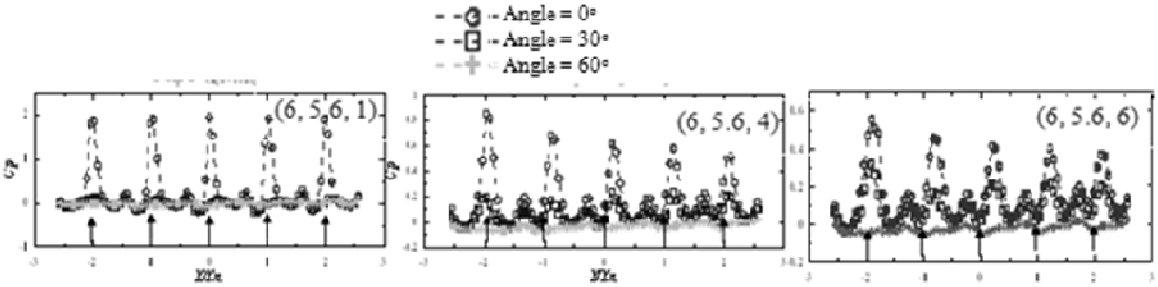

Fig. 9 Influence of jet to jet spacing on the coefficient of pressure (*Cp*) for a given *D/d* and z/*d* at an angle of 0° and a *Re* = 20000

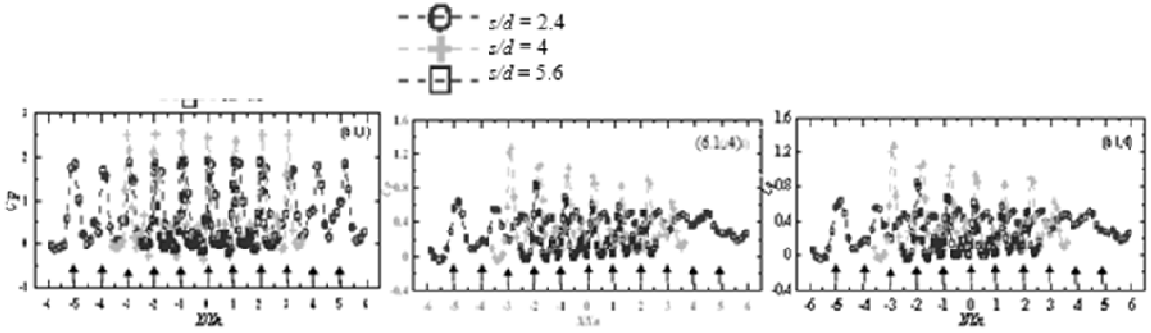

Fig. 10 Speculated figure of jet exit direction

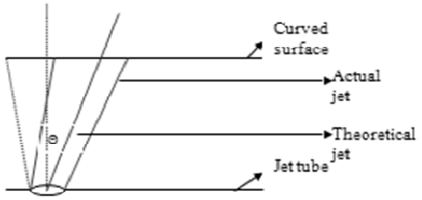

Fig. 11 Phenomenon of upwash and position of secondary peaks.

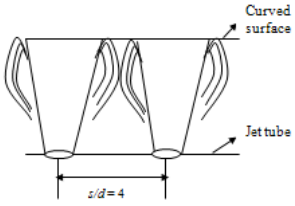

Fig. 11a Upwash as mentioned in [7]

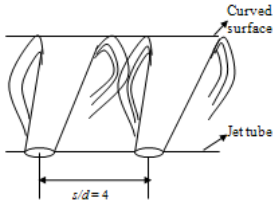

Fig. 11b Speculated figure for upwash to explain the shifts in secondary peaks

Fig. 12 Speculated figure of Jet cone reaching the pressure tap location at 30^{o}

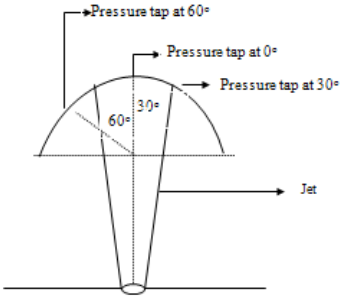

Fig. 12 Speculated figure of Jet cone reaching the pressure tap location at 30°

Fig. 13 Speculated figure for jet mixing phenomenon at lower jet to plate distances

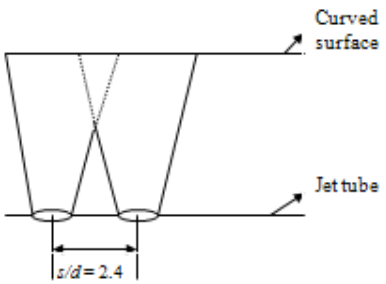

Fig. 13a Mixing of jets for lower jet to jet distances

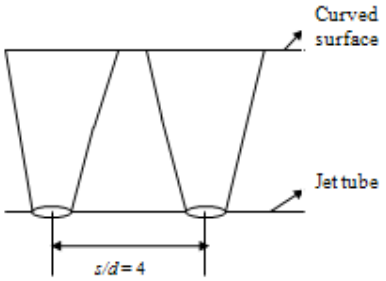

Fig. 13b No mixing phenomenon for a jet to jet distance of 4